New Joint Demosaicing and Arbitrary-Ratio Resizing Algorithm for Color Filter Array Based on DCT Approach

Kuo-Liang Chung, *Senior Member*, IEEE, Wei-Jen Yang, Wen-Ming Yan, and Chiou-Shann Fuh, *Member*, IEEE

Abstract — *This paper presents a new joint demosaicing and arbitrary-ratio resizing algorithm for mosaic images. By using the adaptive heterogeneity projection masks and Sobel- and luminance estimation-based (SL-based) masks, more accurate edge information is extracted first. Next, the fully populated green color plane is constructed by using the edge-sensing approach and color difference idea. Instead of interpolating the R and B color planes directly, the green-red color difference plane and green-blue color difference plane are therefore interpolated in order to reduce the estimation error. Next, based on the discrete cosine transform (DCT) technique, the above three constructed planes are resized to the arbitrary sized ones. Finally, the resized red and blue color planes are constructed by using the three resized planes, and then the arbitrary sized full color image is obtained. To the best of our knowledge, this is the first time that such a joint demosaicing and arbitrary-ratio resizing algorithm for mosaic images is presented. Based on twenty-four popular testing mosaic images, the proposed resizing algorithm has better image quality performance when compared with three native algorithms which are the combinations of three well-know demosaicing methods and one existing resizing method. Thus, the proposed algorithm can be used in consumer electronic products, such as digital cameras and digital camcorders, to provide the quality-efficient arbitrary-ratio resizing effect.* [1]

Index Terms — Arbitrary-ratio resizing algorithm, Color difference, Color filter array, DCT, Demosaicing algorithm, Digital cameras.

I. INTRODUCTION

In order to economize the hardware cost, instead of using three CCD/CMOS sensors, most digital cameras use a single sensor array to capture the color information based on Bayer color filter array (CFA) structure [3] which is depicted in Fig. 1.

[1] This work is supported by the National Science Council of R. O. C. under contract NSC 98-2221-E-011-102-MY3.

Kuo-Liang Chung and Wei-Jen Yang are with the Department of Computer Science and Information Engineering, National Taiwan University of Science and Technology, No. 43, Section 4, Keelung Road, Taipei, Taiwan 10672, R. O. C. (e-mail: {k.l.chung, a9115001}@mail.ntust.edu.tw).

Wen-Ming Yan and Chiou-Shann Fuh are with the Department of Computer Science and Information Engineering, National Taiwan University, No. 1, Section 4, Roosevelt Road, Taipei, Taiwan 10617, R. O. C. (email: {ganboon, fuh}@csie.ntu.edu.tw).

Contributed Paper
Original manuscript received December 16, 2009
Revised manuscript received January 12, 2010
Current version published 06 29 2010;
Electronic version published 07 06 2010.

In Bayer CFA structure, each pixel in the captured image has only one of the three primary colors and this kind of

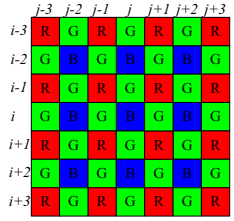

Fig. 1. The Bayer CFA structure.

image is called the mosaic image. Because the green (G) color plane is the most important factor to determine the luminance of the color image, half of the pixels in Bayer CFA structure are assigned to G color plane; the red (R) and blue (B) color planes share the remaining parts evenly.

Since each pixel in the mosaic image has only one color component, the two missing color components for one color pixel should be recovered as best as possible and such a recovering process is called the demosaicing process which has been studied extensively [1], [4], [5], [7], [9], [10], [12], [13], [15], [17], [18], [19], [22], [24], [25], [26], [27]. Besides the demosaicing issue, how to resize mosaic images is another important research issue. The terms "resize" and "zoom" are used exchangeably. Several resizing algorithms for mosaic images have been developed [2], [6], [8], [16], [20], [21], [28] Unfortunately, all of them only focus on the quad-zooming process. The motivation of this research is to develop a new joint demosaicing and arbitrary-ratio resizing algorithm for mosaic images.

In this paper, a new joint demosaicing and arbitrary-ratio resizing algorithm for mosaic images is presented. First, more accurate edge information is extracted from the mosaic image by using the adaptive heterogeneity projection masks and SL-based masks [7]. Next, the fully populated G color plane is constructed by using the edge-sensing approach and color difference idea. Instead of interpolating the R and B color planes directly, the green-red color difference plane and green-blue color difference plane are therefore interpolated in order to reduce the estimation error. Then, based on the composite length DCT technique [23], the three constructed planes can be resized to obtain arbitrary-ratio sized ones. Finally, the resized red and blue color planes are gotten by using the two resized color difference planes and the resized green color plane, and then the arbitrary-ratio resized full color image is followed. The flowchart of the proposed

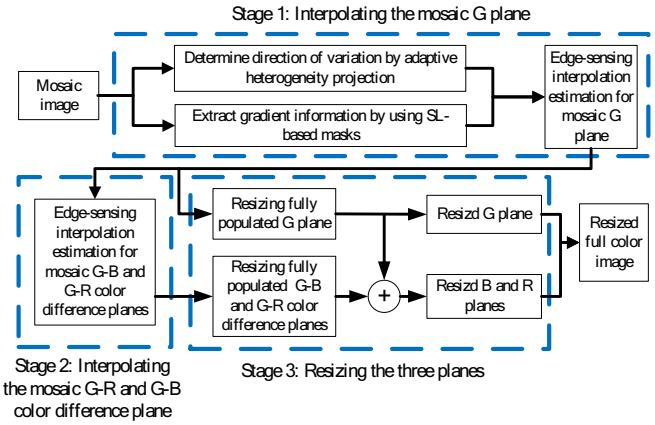

Fig. 2. The flowchart of the proposed arbitrary-ratio resizing algorithm.

resizing algorithm is illustrated in Fig. 2. This is the first time that such a joint demosaicing and arbitrary-ratio resizing algorithm for mosaic images is presented. Based on twenty-four popular testing mosaic images, the proposed algorithm has better image quality performance in terms of two objective color image quality measures, the color peak signal-to-noise ratio (CPSNR) and the S-CIELAB ΔE^*_{ab}, and one subjective color image quality measure, the color artifacts, when compared with three native algorithms which are the combinations of three well-know demosaicing methods [5], [19], [24] and one existing resizing method [23].

The remainder of this paper is organized as follows. In Section II, the adaptive heterogeneity projection masks and SL-based masks, which are used to extract more accurate edge information from mosaic images, are introduced. In Section III, based on the extracted edge information and the composite length DCT, the proposed arbitrary-ratio resizing algorithm for mosaic images is presented. In Section IV, some experimental results are demonstrated to show the quality advantage of the proposed algorithm. Finally, some concluding remarks are addressed in Section V.

II. Extracting More Accurate Edge Information from Mosaic Images

In this section, how to use the adaptive heterogeneity projection masks and the SL-based masks [7] to extract more accurate edge information from mosaic images is introduced. For exposition, the R, G, and B color pixels at position (i, j) in the mosaic image I_{mo} are denoted by $I^r_{mo}(i, j)$, $I^g_{mo}(i, j)$, and $I^b_{mo}(i, j)$, respectively.

Table I.
Four possible heterogeneity projection masks.

N	$M_{hp}(N)$
5	$[1 \ -2 \ 0 \ 2 \ 1]$
7	$[1 \ -4 \ 5 \ 0 \ -5 \ 4 \ -1]$
9	$[1 \ -6 \ 14 \ -14 \ 0 \ 14 \ -14 \ 6 \ -1]$

A. Adaptive heterogeneity projection

Based on the concept of adaptive heterogeneity projection [7], three possible heterogeneity projection masks with different sizes adopted in this paper are shown in Table I where the terms N and $M_{hp}(N)$ denote the mask size and the corresponding heterogeneity projection mask, respectively. Given a mosaic image I_{mo}, the horizontal heterogeneity projection map HP_{H-map} and the vertical heterogeneity projection map HP_{V-map} can be generated by

$$\begin{aligned} HP_{H-map} &= |\, I_{mo} \otimes M_{hp}(N)^T \,| \\ HP_{V-map} &= |\, I_{mo} \otimes M_{hp}(N) \,| \end{aligned} \tag{1}$$

where the symbol "$\otimes$" denotes the 1-D convolution operator; $|\cdot|$ denotes the absolute value operator; the operator "T" denotes the transpose operator. In order to extract more accurate horizontal and vertical edge information and reduce the computation time, the two proper mask sizes $N_H(i, j)$ and $N_V(i, j)$ for each pixel at position (i, j) should be determined. For simplicity, we only describe the determination of $N_H(i, j)$.

The horizontal spectral-spatial correlation (SSC) [24] map is utilized to determine the proper horizontal mask size for each pixel. For the horizontal SSC map, the horizontal SSC value $S_H(i, j)$ at position (i, j) can be calculated by using Eq. (2).

After generating the horizontal SSC map, the proper horizontal mask sizes $N_H(i, j)$ can be determined thereafter. The depiction of the determination for $N_H(i, j)$ is illustrated in Fig. 3 and the procedure of the determination for $N_H(i, j)$ consists of the following three steps:

- **Step 1:** Initially, we set the left boundary $x_l = j - 2$, the right boundary $x_r = j + 2$, the mask size

$$S_H(i,j) = \begin{cases} \left|I^g_{mo}(i,j) - I^r_{mo}(i,j+1)\right| & \text{if the current pixel is G and } i \in \text{odd.} \\ \left|I^g_{mo}(i,j) - I^b_{mo}(i,j+1)\right| & \text{if the current pixel is G and } i \in \text{even.} \\ \left|I^r_{mo}(i,j) - I^g_{mo}(i,j+1)\right| & \text{if the current pixel is } R. \\ \left|I^b_{mo}(i,j) - I^g_{mo}(i,j+1)\right| & \text{if the current pixel is } B. \end{cases} \tag{2}$$

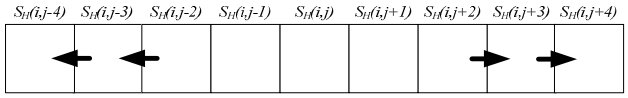

Fig. 3. The depiction of the determination for the proper horizontal mask size $N_H(i,j)$

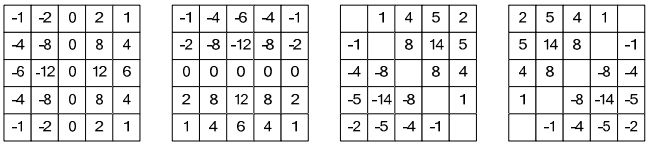

Fig. 4. The four normalized SL-based masks. (a) The horizontal SL-based mask. (b) The vertical SL-based mask. (c) The $\pi/4$-diagonal SL-based mask. (d) The $-\pi/4$-diagonal SL-based mask.

$N_H(i,j)=5,$ and the maximum mask size $N_{max}=9.$

- **Step 2:** If the condition $Max(\Delta S_l,\Delta S_r)<T_h$ where $\Delta S_l=|S_H(i,x_l)-S_H(i,x_l-1)|;\quad \Delta S_r=|S_H(i,x_r)-S_H(i,x_r-1)|;$ $T_h=8$ holds, the mask size $N_H(i,j)$ is output as the proper horizontal mask size. Otherwise, go to Step 3.
- **Step 3:** Update $N_H(i,j),\ x_l,$ and x_r by performing $N_H(i,j)=N_H(i,j)+2,\quad x_l=x_l-1,$ and $x_r=x_r+1,$ respectively. If $N_H(i,j)=N_{max},$ $N_H(i,j)=N_{max}$ is output as the proper mask size and stop the procedure. Otherwise, go to Step 2.

After generating the two heterogeneity projection maps HP_{H-map} and HP_{V-map}, the horizontal and vertical heterogeneity projection values at position (i,j) are denoted by $HP_H(i,j)$ and $HP_V(i,j),$ respectively. Further, the tuned horizontal and vertical heterogeneity projection values can be computed by $HP'_H(i,j)=\sum_{k=-4}^{4}\delta_k HP_H(i,j+k)$ and $HP'_V(i,j)=\sum_{k=-4}^{4}\delta_k HP_V(i+k,j),$ respectively, where $\delta_k=2$ if $k=0;\ \delta_k=1,$ otherwise.

B. SL-based masks for mosaic images

In order to make the Sobel operator workable on mosaic images to extract more accurate gradient information, the luminance estimation technique [1] is embedded into the Sobel operator [11]. The detailed derivations of embedding the luminance estimation technique into the Sobel operator are described in [7]. The four normalized SL-based masks are illustrated in Fig. 4.

By running the above four SL-based masks on the 5×5 mosaic subimage centered at position $(i,j),$ the horizontal gradient response $\Delta I^H_{dm}(i,j),$ the vertical gradient response $\Delta I^V_{dm}(i,j),$ the $\pi/4$-diagonal gradient response $\Delta I^{\pi/4}_{dm}(i,j),$ and the $-\pi/4$-diagonal gradient response $\Delta I^{-\pi/4}_{dm}(i,j)$ can be obtained easily.

III. The Proposed New Joint Demosaicing and Arbitrary-Ratio Resizing Algorithm for Mosaic Images

Our proposed algorithm consists of the following three stages: (1) interpolating the mosaic G plane to construct the fully populated G plane by using the edge-sensing interpolation estimation; (2) interpolating the mosaic G-R and G-B color difference planes to construct the fully populated G-R and G-B color difference planes, respectively; (3) resizing the three constructed planes mentioned above to obtain the arbitrary-ratio sized ones, and then based on the three resized planes, recovering the resized R and B planes to obtain arbitrary-ratio resized full color image.

A. Stage 1: Interpolating the mosaic G plane

In this subsection, the interpolation for the mosaic G plane $I^g_{mo}(i,j)$ to construct the fully populated G plane $I^g_{dm}(i,j)$ by using the edge-sensing approach and color difference idea is presented. For exposition, let us take the central pixel at position (i,j) in Fig. 1 as the representative to explain how to estimate the G color value $I^g_{dm}(i,j)$ from its four neighboring pixels with movement $\Omega_g=\{(x,y)|(x,y)=(i\pm1,j),(i,j\pm1)\}.$ First, according to the tuned horizontal heterogeneity projection value $HP'_H(i,j)$ and the tuned vertical heterogeneity projection value $HP'_V(i,j)$ of the current pixel, three cases, namely the horizontal variation as shown in Fig. 5(a), the vertical variation as shown in Fig. 5(b), and the other variations as shown in Fig. 5(c), are considered in the interpolation estimation phase for $I^g_{mo}(i,j)$. The arrows in Fig. 5 denote the relevant data dependence.

Further, in order to estimate $I^g_{dm}(i,j)$ more accurately, four proper weights in terms of the gradient magnitude are assigned to the corresponding four pixels in the interpolation estimation phase. Given a pixel at position (i,j), based on the horizontal and vertical gradient magnitudes, its horizontal and vertical weights can be determined by $w_g(H,x,y)=1/[1+\sum_{k=-1}^{1}\delta_k\Delta I^H_{dm}(x,y+k)]$ and $w_g(V,x,y)=1/[1+\sum_{k=-1}^{1}\delta_k\Delta I^V_{dm}(x+k,y)],$ respectively, where $\delta_k=3$ if $k=1;\quad \delta_k=1,$ otherwise. Considering the neighboring pixel located at position $(i-1,j),$ if the vertical gradient magnitude is large, i.e. there is a horizontal edge passing through it, based on the color difference assumption [15], [24], it reveals that the G component of this pixel makes less contribution to estimate that of the current pixel; otherwise, it reveals that the G component of this pixel makes more contribution to estimate that of the current pixel. According to the above analysis, the vertical weight

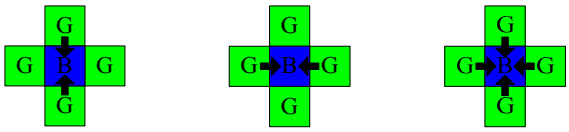

Fig. 5. Data dependence of our proposed interpolation estimation for $I^g_{mo}(i,j)$. (a) Horizontal variation (vertical edge). (b) Vertical variation (horizontal edge). (c) The other variations.

$$w_g(V,i-1,j)=\frac{1}{1+\Delta I^V_{dm}(i,j)+3\Delta I^V_{dm}(i-1,j)+\Delta I^V_{dm}(i-2,j)}.$$ is selected for the pixel at position $(i-1,j)$. By the same argument, the weights of the other three neighbors are selected by $w_g(V,i+1,j)$, $w_g(H,i,j-1)$, and $w_g(H,i,j+1)$, respectively. Consequently, the value of $I^g_{dm}(i,j)$ can be estimated by

$$I^g_{dm}(i,j)=I^b_{mo}(i,j)+\frac{\Sigma_{(d,x,y)\in\xi_g} w_g(d,x,y)D_{gb}(x,y)}{\Sigma_{(d,x,y)\in\xi_g} w_g(d,x,y)}$$

$$\xi_g=\begin{cases}\xi_1 & \text{if } HP'_V(i,j)<\alpha HP'_H(i,j)\\ \xi_2 & \text{if } HP'_H(i,j)<\alpha HP'_V(i,j)\\ \xi_1\cup\xi_2 & \text{Ohterwise}\end{cases} \tag{3}$$

where $\xi_1=\{(V,i\pm1,j)\}$ and $\xi_2=\{(H,i,j\pm1)\}$; for $(d_1,x_1,y_1)\in\xi_1$,

$$D_{gb}(x_1,y_1)=I^g_{mo}(x_1,y_1)-\frac{1}{2}\sum_{k\in\{\pm1\}} I^b_{mo}(x_1+k,y_1);$$ for $(d_2,x_2,y_2)\in\xi_2$,

$$D_{gb}(x_2,y_2)=I^g_{mo}(x_2,y_2)-\frac{1}{2}\sum_{k\in\{\pm1\}} I^b_{mo}(x_2,y_2+k);$$ the parameter α is set to $\alpha=0.55$ empirically.

Finally, a new proposed refinement approach, which combines the concept of the local color ratios [17] and the extracted more accurate edge information, is addressed to refine the fully populated G plane. For the current pixel at position (i,j), its G value $I^g_{dm}(i,j)$ can be refined by the following rule:

$$I^g_{dm}(i,j)=-\beta+(I^b_{mo}(i,j)+\beta)\frac{\sum_{(d,x,y)\in\xi'_g}\delta_{(d,x,y)}w_g(d,x,y)R_{gb}(x,y)}{\sum_{(d,x,y)\in\xi'_g}\delta_{(d,x,y)}w_g(d,x,y)}$$

$$\xi'_g=\begin{cases}\xi'_1 & \text{if } HP'_V(i,j)<\alpha HP'_H(i,j)\\ \xi'_2 & \text{if } HP'_H(i,j)<\alpha HP'_V(i,j)\\ \xi'_1\cup\xi'_2 & \text{Ohterwise}\end{cases} \tag{4}$$

where $\xi'_1=\{(V,i+k,j)\,|\,k\in\{0,\pm2\}\}$; $\xi'_2=\{(H,i,j+k)\,|\,k\in\{0,\pm2\}\}$; $R_{gb}(x,y)=\frac{I^g_{dm}(x,y)+\beta}{I^b_{mo}(x,y)+\beta}$; the parameter β is set to $\beta=256$ empirically.

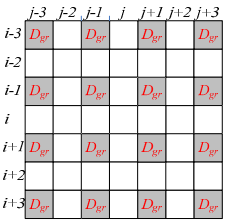

Fig. 6. The pattern of the mosaic G-R color difference plane.

B. Stage 2: Interpolating the mosaic G-R and G-B color difference planes

Instead of interpolating the R and B color planes directly, we interpolate the G-R and G-B color difference planes because the color difference plane is much smoother than the original color plane and it would alleviate the amplification of the estimation error in the later resizing stage. Since the interpolation for G-R color difference plane is the same as that for G-B color difference plane, we only present it for G-R color difference plane consisting of three steps.

In Step 1, according to the mosaic image I^g_{mo} (see Fig. 1) and the fully populated G plane I^g_{dm}, the mosaic G-R plane can be obtained by $D_{gr}(i_r,j_r)=I^g_{dm}(i_r,j_r)-I^r_{mo}(i_r,j_r)$ where $(i_r,j_r)\in\{(i\pm2m+1,j\pm2n+1)\}$. After performing Step 1, Fig. 6 illustrates the pattern of the obtained mosaic G-R color difference plane for the positions depicted in in gray cells. The G-R color difference plane interpolation estimation for the other positions consists of two steps: Step 2: interpolating the G-R color difference values of the pixels at positions $\{(i\pm2m,j\pm2n)\}$ in Fig. 6; Step 3: interpolating the G-R color difference values of the pixels at positions $\{(i\pm2m,j\pm2n+1)\}$ and $\{(i\pm2m+1,j\pm2n)\}$.

For simplicity, the central pixel at position (i,j) in Fig. 6 is taken as the representative to explain the G-R color difference plane interpolation performed in Step 2. The G-R color difference value $D_{gr}(i,j)$ can be estimated from its four neighboring pixels, which have been interpolated in last subsection, with movement $\Omega_r=\{(x,y)\,|\,(x,y)=(i\pm1,j\pm1)\}$. In order to estimate $D_{gr}(i,j)$ more accurately, the gradient magnitudes of four diagonal variations are considered to determine the proper four weights. Given a pixel at position (x,y), its $-\pi/4$-diagonal and $\pi/4$-diagonal weights can be determine by $w_{gr}(-\pi/4,x,y)=1/[1+\sum_{k=-1}^{1}\delta_k\Delta I^{-\pi/4}_{dm}(x+k,y+k)]$ and $w_{gr}(\pi/4,x,y)=1/[1+\sum_{k=-1}^{1}\delta_k\Delta I^{\pi/4}_{dm}(x-k,y+k)]$ respectively, where $\delta_k=3$ if $k=1$; $\delta_k=1$, otherwise. Thus, the four weights of the four diagonal neighbors of the current pixel at position (i,j) are denoted by $w_{gr}(-\pi/4,i-1,j-1)$, $w_{gr}(\pi/4,i-1,j+1)$, $w_{gr}(\pi/4,i+1,j-1)$, and

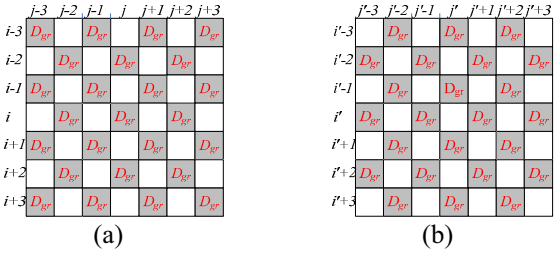

Fig. 7. Two patterns of the G-R color difference plane. (a) The pattern of the G-R color difference plane after performing Step 1. (b) The pattern shifting (a) one pixel down.

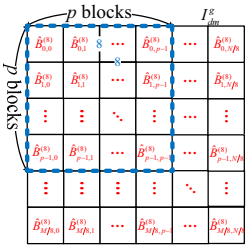

Fig. 8. An example of the active unit in $\hat{\Phi}_{I^g_{dm}}$.

$w_{gr}(-\pi/4, i+1, j+1)$, respectively. Based on the four weights, the G-R color difference value at position (i, j) can be estimated by

$$D_{gr}(i,j) = \frac{\sum_{(d,x,y)\in\xi_{gr}} w_{gr}(d,x,y) D_{gr}(x,y)}{\sum_{(d,x,y)\in\xi_{gr}} w_{gr}(d,x,y)} \tag{5}$$

where $\xi_{gr} = \{(-\pi/4, i-1, j-1), (\pi/4, i-1, j+1), (\pi/4, i+1, j-1), (-\pi/4, i+1, j+1)\}$.

After performing Step 2, the current pattern of the G-R color difference plane is illustrated in Fig. 7(a). For easy exposition, the central pixel at position (i', j') in Fig. 7(b), which is obtained by shifting Fig. 7(a) one pixel down, is taken as the representative to explain the G-R color difference plane interpolation in Step 2. Referring to Fig. 7(b), it is not hard to find that the pattern of the G-R color difference plane at present is the same as that of the G plane in the mosaic image as shown in Fig. 1. Therefore, the interpolation estimation approach described in last subsection can be directly used to estimate the G-R color difference value at position (i', j'). Consequently, the G-R color difference value of the current pixel can be estimated by

$$D_{gr}(i,j) = \frac{\sum_{(d,x,y)\in\xi'_{gr}} w_{gr}(d,x,y) D_{gr}(x,y)}{\sum_{(d,x,y)\in\xi'_{gr}} w_{gr}(d,x,y)}$$

$$\xi'_g = \begin{cases} \xi_1 & \text{if } HP'_V(i,j) < \alpha HP'_H(i,j) \\ \xi_2 & \text{if } HP'_H(i,j) < \alpha HP'_V(i,j) \\ \xi_1 \cup \xi_2 & \text{Ohterwise} \end{cases} \tag{6}$$

where $\xi_1 = \{(V, i\pm1, j)\}$ and $\xi_2 = \{(H, i, j\pm1)\}$; $w_{gr}(H,x,y) = 1/[1+\sum_{k=-1}^{1} \delta_k \Delta I^H_{dm}(x, y+k)]$ and $w_{gr}(V,x,y) = 1/[1+\sum_{k=-1}^{1} \delta_k \Delta I^V_{dm}(x+k, y)]$ where $\delta_k = 3$ if $k = 1$; $\delta_k = 1$, otherwise; the parameter α is set to $\alpha = 0.55$ empirically.

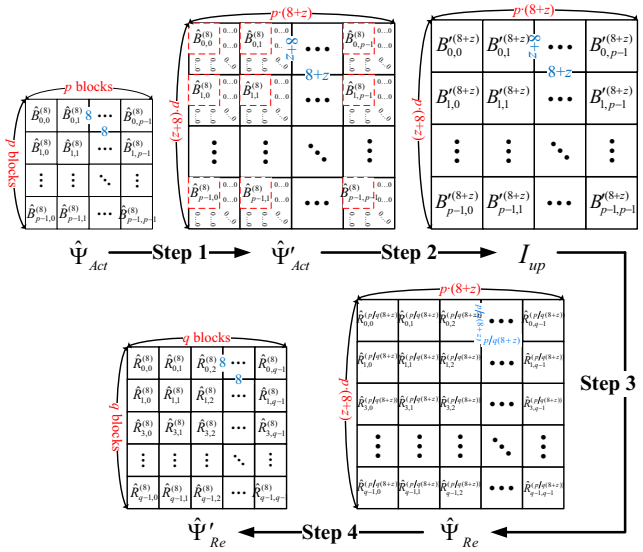

Fig. 9. The depiction of the q/p -fold resizing procedure.

After constructing the fully populated G plane, G-R color difference plane, and G-B color difference plane, in next subsection, the three constructed planes will be resized to the arbitrary-ratio sized ones by using the DCT approach, and then the arbitrary-ratio resized full color image is followed.

C. Stage 3: Resizing the fully populated G plane, G-R color difference plane, and G-B color difference plane

Based on the composite length DCT [23], this subsection presents the arbitrary-ratio resizing stage for constructing the fully populated G plane I^g_{dm}, G-R color difference plane D_{gr}, and G-B color difference plane D_{gb}. Since the resizing stage for I^g_{dm} is the same as that for D_{gr} and D_{gb}, we only present it for I^g_{dm}. Let $DCT(B^{(a)})$ and $IDCT(B^{(a)})$ be the DCT and inverse DCT on the $a\times a$ block $B^{(a)}$. For the fully populated G plane I^g_{dm}, with size $M\times N$, we first divide it into a set of the image blocks, each with size 8×8, and the obtained image block set is denoted by $\Phi_{I^g_{dm}} = \{B^{(8)}_{m.n} \mid 0 \le m \le \frac{M}{8}-1, 0 \le n \le \frac{N}{8}-1\}$ where $B^{(8)}_{m.n}$ denotes the $(\frac{mN}{8}+n)$-th block in $\Phi_{I^g_{dm}}$. Then, the DCT is performed on each 8×8 image block to obtain the set of transformed blocks, $\hat{\Phi}_{I^g_{dm}} = \{\hat{B}^{(8)}_{m.n} \mid 0 \le m \le \frac{M}{8}-1, 0 \le n \le \frac{N}{8}-1\}$. If we want to resize the $M\times N$ G plane I^g_{dm} to the one with size $q/p\,M \times q/p\,N$ the resizing ratio is said to q/p. According to the resizing ratio q/p, first p^2 blocks in $\hat{\Phi}_{I^g_{dm}}$ are collected to be an active unit which are surrounded by dashed lines in Fig. 8. In order to achieve resizing ratio q/p, the p^2 blocks

Fig. 10. The twenty-four testing images from Kodak PhotoCD.

In each active unit should be increased or decreased to q^2 blocks.

For the active unit $\hat{\psi}_{Act} = \{\hat{B}^{(8)}_{m.n} \mid 0 \le m,n \le p-1\}$, the q/p-fold resizing procedure consists of the following four steps and the resizing procedure is depicted in Fig. 9.

- **Step 1:** Each 8×8 DCT coefficient block $\hat{B}^{(8)}_{m.n}$ in the active unit is expanded to a $(8+z)\times(8+z)$ block $\hat{B}'^{(8+z)}_{m,n}$ by the following zero padding rule:

$$\hat{B}'^{(8+z)}_{m,n}(x,y) = \begin{cases} \hat{B}^{(8)}_{m.n}(x,y) & \text{if } 0 \le x,y<8 \\ 0 & \text{otherwise} \end{cases} \quad (7)$$

$$\forall x,y \in \{0,1,\ldots,z-1\};\ \forall m,n \in \{0,1,\ldots,p-1\}$$

where z denotes the smallest nonnegative integer satisfying the condition: $p(8+z) = Cq,\quad C \ge 8$. For example, assume $q/p = 4/3$ then the smallest z is 4 due to $3(8+4) = 9\times 4$. Consequently, we have the set of zero padded DCT coefficient blocks $\hat{\psi}'_{Act} = \{\hat{B}'^{(8+z)}_{m,n} \mid 0 \le m,n \le p-1\}$.

- **Step 2:** For each $\hat{B}'^{(8+z)}_{m,n}$ in $\hat{\psi}'_{Act}$, the $(8+z)\times(8+z)$ IDCT is performed on it to obtain the upsized image:

$$B'^{(8+z)}_{m,n} = IDCT(\hat{B}'^{(8+z)}_{m,n}) \quad (8)$$

After performing the $(8+z)\times(8+z)$-sample IDCT's on all the zero padded DCT coefficient blocks in $\hat{\psi}'_{Act}$, the upsized subimage I_{up} $(=\bigcup_{0\le m,n\le p-1} B'^{(8+z)}_{m,n})$ is constructed.

- **Step 3:** Then, the upsized subimage I_{up} is divided into q^2 blocks, each block with size $q/p(8+z)\times q/p(8+z)$, and the set of the resampled image blocks is denoted by $\psi_{\mathrm{Re}} = \{R^{(\frac{q}{p}(8+z))}_{m,n} \mid 0 \le m,n \le p-1\}$. Next, the DCT is performed on each $R^{(\frac{q}{p}(8+z))}_{m,n}$ to construct the resampled DCT coefficient block $\hat{R}^{(\frac{q}{p}(8+z))}_{m,n}$ by

$$\hat{R}^{(\frac{q}{p}(8+z))}_{m,n} = DCT(R^{(\frac{q}{p}(8+z))}_{m,n}),\ 0 \le m,n \le q-1 \quad (9)$$

TABLE II.
AVERAGE CPSNR COMPARISON FOR THE FOUR CONCERNED ALGORITHMS.

	Resizing ratio q/p				
	2	8/5	4/3	8/7	Average
A_1	28.4051	30.2171	32.1575	34.1260	31.2264
A_2	28.4107	30.1089	31.8667	33.6307	31.0043
A_3	28.6069	30.5344	32.5719	34.6149	31.5820
Ours	**29.1714**	**31.3134**	**33.6423**	**35.8527**	**32.4950**

TABLE III.
AVERAGE S-CIELAB ΔE^*_{ab} COMPARISON FOR THE FOUR CONCERNED ALGORITHMS.

	Resizing ratio q/p				
	2	8/5	4/3	8/7	Average
A_1	3.52927	3.05053	2.62441	2.17526	2.84487
A_2	3.50429	3.09378	2.74100	2.35818	2.92431
A_3	3.41551	2.92146	2.50336	2.07863	2.72974
Ours	**3.17182**	**2.70866**	**2.32772**	**2.00323**	**2.55286**

We thus have the set of resampled DCT coefficient blocks $\hat{\psi}_{\mathrm{Re}} = \{\hat{R}^{(\frac{q}{p}(8+z))}_{m,n} \mid 0 \le m,n \le p-1\}$.

- **Step 4:** Finally, the high-frequency DCT coefficients of each block in $\hat{\psi}_{\mathrm{Re}}$ are truncated by the following rule:

$$\hat{R}^{(8)}_{m,n}(x,y) = \hat{R}^{(\frac{q}{p}(8+z))}_{m,n}(x,y)$$
$$\forall x,y \in \{0,1,\ldots,7\};\ \forall m,n \in \{0,1,\ldots,q-1\} \quad (10)$$

where $\hat{R}^{(8)}_{m,n}$ denotes the left-upper 8×8 subblock of $\hat{R}^{(\frac{q}{p}(8+z))}_{m,n}$; $\hat{R}^{(\frac{q}{p}(8+z))}_{m,n}(x,y)$ and $\hat{R}^{(8)}_{m,n}(x,y)$ denote the DCT coefficients of the pixels at position (x,y) in $\hat{R}^{(\frac{q}{p}(8+z))}_{m,n}$ and $\hat{R}^{(8)}_{m,n}$, respectively. Consequently, the resized active unit $\hat{\psi}'_{\mathrm{Re}} = \{\hat{R}'^{(8)}_{m,n} \mid 0 \le m,n \le q-1\}$ is constructed.

After performing the above resizing procedure on all the active units in I^g_{dm}, a set of 8×8 DCT coefficient blocks $\hat{\Phi}_{Z^g_{dm}} = \{\hat{B}^{(8)}_{m.n} \mid 0 \le m \le \frac{q/p\,M}{8}-1, 0 \le n \le \frac{q/p\,N}{8}-1\}$. can be obtained. Consequently, the $q/p\,M \times q/p\,N$ sized G plane Z^g_{dm} can be obtained by performing the IDCT on each 8×8 DCT coefficient blocks in $\hat{\Phi}_{Z^g_{dm}}$. By the same argument, the $q/p\,M \times q/p\,N$ sized G-R and G-B color difference planes, which are denoted by ZD_{gr} and ZD_{gr}, respectively, can be

Fig. 11. The magnified subimage cut from the original testing image No. 8.

Fig. 12. For image No. 8, when the resizing ratio q/p is 2, four magnified subimages cut from the resized images obtained by (a) A_1, (b) A_2, (c) A_3, and (d) the proposed algorithm.

Fig. 13. For image No. 8, when the resizing ratio q/p is $8/5$, four magnified subimages cut from the resized images obtained by (a) A_1, (b) A_2, (c) A_3, and (d) the proposed algorithm.

Fig. 14. For image No. 8, when the resizing ratio q/p is $4/3$, four magnified subimages cut from the resized images obtained by (a) A_1, (b) A_2, (c) A_3, and (d) the proposed algorithm.

Fig. 15. For image No. 8, when the resizing ratio q/p is $8/7$, four magnified subimages cut from the resized images obtained by (a) A_1, (b) A_2, (c) A_3, and (d) the proposed algorithm.

also obtained. Finally, the $q/p\,M \times q/p\,N$ sized R and B planes can be constructed by

$$\begin{aligned} Z^r_{dm}(i_z,j_z) &= Z^g_{dm}(i_z,j_z) - ZD_{gr}(i_z,j_z) \\ Z^b_{dm}(i_z,j_z) &= Z^g_{dm}(i_z,j_z) - ZD_{gb}(i_z,j_z) \end{aligned} \tag{11}$$

where $Z^r_{dm}(i_z,j_z)$, $Z^g_{dm}(i_z,j_z)$, and $Z^b_{dm}(i_z,j_z)$ denote the three color components of the pixel at position (i_z,j_z) in the $q/p\,M \times q/p\,N$ sized full color image Z_{dm}, respectively; $ZD_{gr}(i_z,j_z)$ and $ZD_{gb}(i_z,j_z)$ denote the G-R and G-B color difference value of the pixel at position (i_z,j_z) in ZD_{gr} and ZD_{gb}, respectively.

IV. Experimental Results

In this section, based on twenty-four popular testing mosaic images, some experimental results are demonstrated to show the applicability and quality advantages of the proposed algorithm. Fig. 10 illustrates the twenty-four testing images from Kodak PhotoCD [29]. In our experiments, the twenty-four testing images, each with size 512×768, are first downsized to the $q/p\,512\times q/p\,768$ sized ones by using the resizing method proposed in [23], and then the downsized images are down-sampled to the mosaic images.

In order to evaluate the performance of the proposed joint demosaicing and resizing algorithm, three native resizing algorithms for mosaic images are adopted to compare with the proposed algorithm. In the three native resizing algorithms, one of the three demosaicing methods proposed in [24], [19], and [5], respectively, is first utilized to obtain the demosaiced images and then the resizing method proposed in [23] is applied to construct the resized full color images. In addition, the postprocessing approach proposed in [17] is adopted to the three concerned demosaicing methods to enhance the demosaiced image quality. For convenience, the three native algorithms based on the demosaicing methods proposed in [24], [19], and [5] are called A_1, A_2, and A_3, respectively. The concerned algorithms are implemented on the IBM compatible computer with Intel Core 2 Duo CPU 1.83GHz and 2GB RAM. The operating system used is MS-Windows XP and the program developing environment is Borland C++ Builder 6.0. Further, the concerned results are available in [30].

Here, we adopt two objective color image quality measures, the CPSNR and the S-CIELAB ΔE^*_{ab} [14],[15], and one subjective color image quality measure, the color artifacts, to justify the quality advantage of the proposed algorithm. The CPSNR for a color image with size $M\times N$ is defined by

$$\text{CPSNR}=10\log_{10}\frac{255^2}{\frac{1}{3MN}\sum_{m=0}^{M-1}\sum_{n=0}^{N-1}\sum_{c\in C}\left[I^c_{ori}(m,n)-Z^c_{dm}(m,n)\right]^2} \tag{12}$$

where $C\in\{r,g,b\}$; $I^r_{ori}(m,n)$, $I^g_{ori}(m,n)$, and $I^b_{ori}(m,n)$ denote the three color components of the color pixel at position (m,n) in the original full color image; $Z^r_{dm}(m,n)$, $Z^g_{dm}(m,n)$, and $Z^b_{dm}(m,n)$ denote the three color components of the color pixel at position (i,j) in the zoomed full color image. The greater the CPSNR is, the better the image quality is. The S-CIELAB ΔE^*_{ab} of a color image with size $M\times N$ is defined by

$$\Delta E^*_{ab}=\frac{1}{MN}\sum_{m=0}^{M-1}\sum_{n=0}^{N-1}\left\{\sqrt{\sum_{c\in\Gamma}EI^c_{ori}(m,n)-EZ^c_{dm}(m,n)}\right\} \tag{13}$$

where $\Gamma \in \{L,a,b\}$; $EI^{L}_{ori}(m,n)$, $EI^{a}_{ori}(m,n)$, and $EI^{b}_{ori}(m,n)$ denote the three CIELAB color components of the color pixel at position (m,n) in the original full color image; $EZ^{L}_{dm}(m,n)$, $EZ^{a}_{dm}(m,n)$, and $EZ^{b}_{dm}(m,n)$ denote the three CIELAB color components of the color pixel at position (m,n) in the resized full color image. The smaller the S-CIELAB ΔE^{*}_{ab} is, the better the image quality is.

Based on twenty-four testing images, among the four concerned resizing algorithms, Table I and Table II demonstrate the image quality comparison in terms of the average CPSNR and the average S-CIELAB ΔE^{*}_{ab}, respectively. In Table I and Table II, the entries with the largest CPSNR and the smallest S-CIELAB ΔE^{*}_{ab} are highlighted by boldface. From Table I and Table II, it is observed that the proposed resizing algorithm produces the best image quality in terms of CPSNR and S-CIELAB ΔE^{*}_{ab} among the four algorithms.

Next, the subjective image visual measure, color artifacts, is adopted to demonstrate the visual quality advantage of the proposed resizing algorithm. Some color artifacts may appear on nonsmooth regions of the full color image after demosaicing and resizing the mosaic image. In order to examine the color artifacts among the concerned algorithms, the magnified subimages containing nonsmooth contents in the resized full color images are cut off. First, seventeen magnified subimages cut from the testing image No. 8 are adopted to examine the visual effect among the four concerned algorithms. Fig. 11 illustrates the magnified subimage cut from the original testing image No. 8. Based on different resizing ratios, Fig. 12-Fig. 15 illustrate magnified subimages cut from the resized images obtained by the four concerned resizing algorithms. From the visual comparison, it is observed that based on the same resizing ratio, the proposed algorithm produces less color artifacts when compared with the other three algorithms. We take the magnified subimages cut from the testing image No. 23 for the visual comparison and Fig. 16-Fig. 20 illustrate the concerned magnified subimages. Similar to the color artifact examination for image No. 8, it is observed that the proposed resizing algorithm produces the least color artifacts, i.e. the best visual effect. More visual results of the concerned algorithms are available in [30].

Finally, based on twenty-four testing mosaic images and four resizing ratios, the average execution-time of the four concerned resizing algorithms are shown in Table IV. It is observed that the average execution-time of the proposed resizing algorithm is moderate when compared with the other three algorithms. However, the proposed algorithm has the best image quality performance in the four resizing algorithms.

Fig. 16. The magnified subimage cut from the original testing image No. 23.

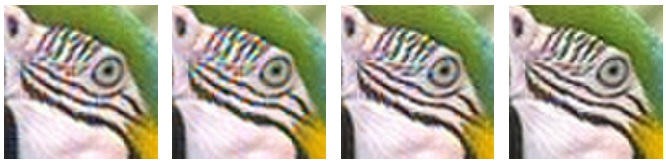

(a) (b) (c) (d)

Fig. 17. For image No. 23, when the resizing ratio q/p is 2, four magnified subimages cut from the resized images obtained by (a) A_1, (b) A_2, (c) A_3, and (d) the proposed algorithm.

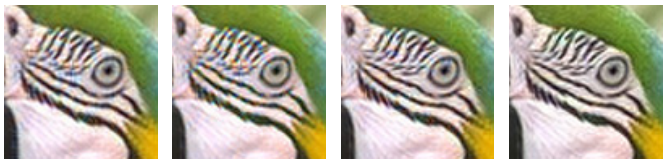

(a) (b) (c) (d)

Fig. 18. For image No. 23, when the resizing ratio q/p is $8/5$, four magnified subimages cut from the resized images obtained by (a) A_1, (b) A_2, (c) A_3, and (d) the proposed algorithm.

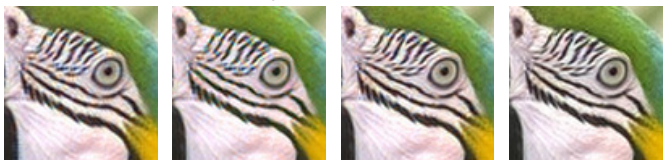

(a) (b) (c) (d)

Fig. 19. For image No. 23, when the resizing ratio q/p is $4/3$, four magnified subimages cut from the resized images obtained by (a) A_1, (b) A_2, (c) A_3, and (d) the proposed algorithm.

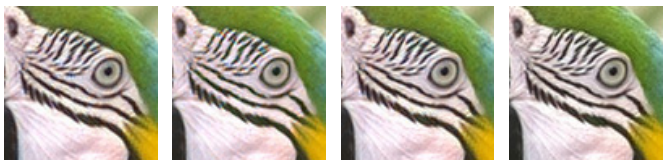

(a) (b) (c) (d)

Fig. 20. For image No. 23, when the resizing ratio q/p is $8/7$, four magnified subimages cut from the resized images obtained by (a) A_1, (b) A_2, (c) A_3, and (d) the proposed algorithm..

V. Conclusions

In this paper, a new joint demosaicing and arbitrary-ratio resizing algorithm for mosaic images has been presented. Based on the color difference concept and the composite length DCT, the mosaic image can be demosaiced and resized to an arbitrary-ratio sized full color image. To the best of our knowledge, this is the first time that such a joint demosaicing

Table IV.
Average execution time of the four concerned algorithms.

Algorithm	A_1	A_2	A_3	*Ours*
Time(s)	12.52	12.94	12.68	12.76

and arbitrary-ratio resizing algorithm for the mosaic image is presented. Based on twenty-four popular testing mosaic images, the proposed new resizing algorithm has better image quality performance when compared with three native algorithms which are the combinations of three well-know demosaicing methods and one existing resizing method. Consequently, the proposed algorithm can be utilized in consumer electronic products, such as digital cameras and digital camcorders, to provide the higher quality arbitrary-ratio resizing effect when compared with the possibility of doing the demosaicing process and the resizing process separately.

REFERENCES

[1] D. Alleysson, S. Susstrunk, and J. Herault, "Linear demosaicing inspired by the human visual system," *IEEE Trans. Image Processing*, vol. 14, no. 4, pp. 439-449, 2005.

[2] S. Battiato, G. Gallo, and F. Stanco, "A locally adaptive zooming algorithm for digital images," *Image and Vision Computing,* vol. 20, no. 11, pp. 805-812, 2002.

[3] B. E. Bayer, "Color imaging array," U.S. Patent # 3 971 065, 1976

[4] H. A. Chang and H. H. Chen, "Stochastic color interpolation for digital cameras," *IEEE Trans. Circuits and Systems for Video Technology,* vol. 17, no. 8, pp. 964-973, 2007.

[5] K. H. Chung and Y. H. Chan, "Color demosaicking using variance of color differences," *IEEE Trans. Image Processing,* vol. 15, no. 10, pp. 2944-2955, 2006.

[6] K. H. Chung and Y. H. Chan, "A low-complexity joint color demosaicking and zooming algorithm for digital camera," *IEEE Trans. Image Processing,* vol. 16, no. 7, pp. 1705-1715, 2007

[7] K. L. Chung, W. J. Yang, W. M. Yan, and C. C. Wang, "Demosaicing of color filter array captured images using gradient edge detection masks and adaptive heterogeneity-projection," *IEEE Trans. Image Processing,* vol. 17, no. 12, pp. 2356-2367, 2008.

[8] K. L. Chung, W. J. Yang, P. Y. Chen, W. M. Yan, and C. S. Fuh, "New joint demosaicing and zooming algorithm for color filter array," *IEEE Trans. Consumer Electronics,* vol. 55, no. 3, pp.1477-1486, 2009.

[9] D. R. Cok, "Signal processing method and apparatus for producing interpolated chrominance values in a sampled color image signal," U.S. Patent # 4 642 678, 1987

[10] E. Dubois, "Frequency-domain methods for demosaicking of bayer-sampled color images," *IEEE Signal Processing Letters,* vol. 12, no. 12, pp. 847-850, 2005.

[11] R. Gonzalez and R. Woods, Digital Image Processing, Addison Wesley, New York, 1992.

[12] B. Gunturk, Y. Altunbasak, and R. Mersereau, "Color plane interpolation using alternating projections," *IEEE Trans. Image Processing,* vol. 11, no. 9, pp. 997-1013, 2002.

[13] H. Hibbard, "Apparatus and method for adaptively interpolating a full color image utilizing luminance gradients," U.S. Patent # 5 382 976, 1995.

[14] R. W. G. Hunt, Measuring Colour, 2nd Ed., Ellis Horwood, Chichester, U.K., 1995.

[15] W. Lu and Y. P. Tang, "Color filter array demosaicking: new method and performance measures," *IEEE Trans. Image Processing,* vol. 12, no. 10, pp. 1194-1210, 2003.

[16] R. Lukac and K. N. Plataniotis, "Digital camera zooming on the color filter array," *Electronics Letters,* vol. 39, no. 25, pp. 1806-1807, 2003.

[17] R. Lukac, K. Martin, and K. N. Plataniotis, "Demosaicked image postprocessing using local color ratios," *IEEE Trans. Circuits and Systems for Video Technology,* vol. 14, no. 6, pp. 914-920, 2004.

[18] R. Lukac, K. N. Plataniotis, D. Hatzinakos, and M. Aleksic, "A novel cost effective demosaicing approach," *IEEE Trans. Consumer Electronics,* vol. 50, no. 1, pp. 256-261, 2004.

[19] R. Lukac and K. N. Plataniotis, "Normalized color-ratio modeling for CFA interpolation," *IEEE Trans. Consumer Electronics,* vol. 50, no. 2, pp. 737-745, 2004.

[20] R. Lukac, K. N. Plataniotis, and D. Hatzinakos, "Color image zooming on the Bayer pattern," *IEEE Trans. Circuits and Systems for Video Technology,* vol. 15, no. 11, pp. 1475-1492, 2005.

[21] R. Lukac and K. N. Platataniotis, "Digital zooming for color filter array," *Real-Time Imaging,* vol. 11, no. 2, pp. 129-138, 2005.

[22] D. D. Muresan and T. W. Parks, "Demosaicing using optimal recovery," *IEEE Trans. Image Processing,* vol. 14, no. 2, pp. 267-278, 2005.

[23] Y. S. Park and H. W. Park, "Arbitrary-ratio image resizing using fast DCT of composite length for DCT-based transcoder," *IEEE Trans. Image Processing,* vol. 15, no. 2, pp. 494-500, 2006.

[24] S. C. Pei and I. K. Tam, "Effective color interpolation in CCD color filter arrays using signal correlation," *IEEE Trans. Circuits and Systems for Video Technology,* vol. 13, no. 6, pp. 503-513, 2003.

[25] H. J. Trussell and R. E. Hartwig, "Mathematics for demosaicking," *IEEE Trans. Image Processing,* vol. 11, no. 4, pp. 485-492, 2002.

[26] X. Wu and N. Zhang, "Primary-consistent soft-decision color demosaicing for digital cameras (patent pending)," *IEEE Trans. Image Processing,* vol. 13, no. 9, pp. 1263-1274, 2004.

[27] L. Zhang and X. Wu, "Color demosaicking via directional linear minimum mean square-error interpolation," *IEEE Trans. Image Processing,* vol. 14, no. 12, pp. 2167-2178, 2005.

[28] L. Zhang and D. Zhang, "A joint demosaicking-zooming scheme for single chip digital color cameras," Computer Vision and Image Understanding, vol. 107, no. 1-2, pp. 14-25, 2007.

[29] [Online]Available:http://www.site.uottawa.ca/~edubois/demosaicking/.

[30] [Online]Available:http://140.118.175.164/WJYang/paper/AResizeCFA/.

BIOGRAPHIES

Kuo-Liang Chung (M'91-SM'01) received the B.S., M.S. and Ph.D. degrees in Computer Science and Information Engineering (CSIE) from the National Taiwan University, Taiwan, R.O.C., in 1982, 1984, and 1990, respectively. He was a Visiting Scholar at University of Washington in summer 1999. He was the Head of the Department of CSIE at the National Taiwan University of Science and Technology (NTUST) from 2003 to 2006. He was the Executive Editor of the Journal of the Chinese Institute of Engineers from 1996 to 1998. He received the Distinguished Engineering Professor Award from Chinese Institute of Engineers in 2001; the Distinguished Research Award in 2004 and Distinguished Scholar Research Project Award in 2009 from the National Science Council, Taiwan; the best paper award from the Society of Computer Vision, Graphics, and Image Processing (Taiwan) in 2007; an IET Fellow in 2009, and the University Chair Professor position at NTUST in 2009. His research interests include image processing and compression, and multimedia applications.

Wei-Jen Yang received the B.S. degree in Computer Science and Information Engineering from National Taiwan University of Science and Technology, Taipei, Taiwan, in 2004 and the Ph.D. degree in Computer Science and Information Engineering from National Taiwan University, Taipei, Taiwan, in 2009. His research interests include color image processing, digital camera image processing and compression, computer vision, and pattern recognition.

Wen-Ming Yan received the B.S. and M.S. degrees in Mathematics from National Taiwan University, Taipei, Taiwan. He is now an Associate Professor in Computer Science and Information Engineering at National Taiwan University. His research interests include scientific computation, and image compression and processing.

Chiou-Shann Fuh (S'89-M'95) received the B.S. degree in Computer Science and Information Engineering from National Taiwan University, Taipei, Taiwan, R.O.C., in 1983, the M.S. degree in Computer Science from The Pennsylvania State University, University Park, in 1987, and the Ph.D. degree in Computer Science from Harvard University, Cambridge, MA, in 1992. He was with AT&T Bell Laboratories, Murray Hill, NJ, U.S.A. from 1992 to 1993. He is now a Professor in the Department of Computer Science and Information Engineering at National Taiwan University, Taipei, Taiwan. His research interests include image processing, computer vision, and pattern recognition.